Morphology, Dynamic Mechanical, and Electrical Properties of Bio-Based Poly(trimethylene terephthalate) Blends, Part 1: Poly(trimethylene terephthalate)/ Poly(ether esteramide)/Polyethylene Glycol 400 Bis(2-ethylhexanoate) Blends

Toshikazu Kobayashi,[1] Barbara A. Wood,[2] Gregory S. Blackman,[2] Akio Takemura[3]

[1]*Engineering Polymers, DuPont Co., Wilmington, Delaware 19880-0323*
[2]*Central Research and Development, DuPont Co., Wilmington, Delaware 19880-0323*
[3]*Laboratory of Polymeric Materials, Department of Biomaterial Sciences, Graduate School of Agricultural and Life Sciences, University of Tokyo, Bunkyo-ku, Tokyo 113-8567, Japan*

Received 15 July 2010; accepted 3 October 2010
DOI 10.1002/app.33498
Published online 14 February 2011 in Wiley Online Library (wileyonlinelibrary.com).

ABSTRACT: Bio-based PTT and PTT blends with PEEA of two different ion contents (275 ppm Na and 3515 ppm Na) and PEG 400 bis (2-ethylhexanoate) were prepared by melt processing. The blends were characterized by differential scanning calorimetry, dynamic mechanical analysis, transmission electron microscopy, and atomic force microscopy. Electro-static performance was also investigated for those PTT blends since PEEA is known as an ion conductive polymer. Here we confirmed that PEG 400 bis (2-ethylhexanoate) improves the static decay performance of PTT/PEEA blends. DMA strongly suggests that PEG 400 bis (2-ethylhexanoate) and PEEA are miscible pairs, and PEG 400 bis (2-ethylhexanoate) selectively goes into the PEEA phase rather than the PTT phase, which lowers the T_g of PEEA. Besides topographic analysis of morphology and phase separation, tunneling atomic force microscopy was also applied to see if we can observe the surface directly for the static dissipative material. © 2011 Wiley Periodicals, Inc. J Appl Polym Sci 120: 3519–3529, 2011

Key words: bio-based; PTT; static dissipative; ion conductive polymer; morphology; tunneling AFM

INTRODUCTION

Poly(trimethylene terephthalate) (PTT) is a newly commercialized aromatic semicrystalline polyester with growing applications in fibers, films, and engineering polymers. PTT belongs to the thermoplastic aromatic polyester family, which includes poly (ethylene terephthalate) (PET) and poly(butylene terephthalate) (PBT). DuPont has recently commercialized the Sorona® PTT renewably sourced polymer which is made by polycondensation as shown in Scheme 1 from 1,3-propanediol (derived from renewable corn sugar) and fossil fuel derived terephthalic acid (TPA) or dimethyl terepthalate (DMT). The diol component of this polymer, 1,3-propanediol, can be manufactured via a biological fermentation process from corn sugar.[1–4] DuPont and Genencor International have developed a bacterial biocatalyst to convert corn-derived glucose to 1,3-propanediol in a single stage. DuPont and Tate and Lyle have developed the commercial scale manufacturing process for 1,3-propanediol based on this biocatalyst.

Bio-based polymers are generating considerable interest as alternatives to traditional petroleum based polymers. The polymers and materials derived from mixed sources of renewables and fossil fuels not only have the desired performance but also are drawing a lot of attention from the sustainability point of view.

PTT provides all the advantages generally associated with polyesters, including excellent physical and chemical properties, dimensional stability, low moisture absorption, processability with appropriate nucleating agent, and recyclability. Before DuPont introduced bio-based PTT into the market, petroleum-based PTT was commercially available from 1988 to 2009 from Shell Corp. PTT polymer has been widely studied especially with regard to its fiber properties,[5–8] crystal structure,[9–12] and thermal and crystallization behaviors.[13–19] More recently PTT/clay nanocomposites,[20–23] PTT/carbon nanotube,[24] and polymer blends such as PTT/PET,[25–27] PTT/PBT,[26,28] PTT/PC,[29–32] PTT/EPDM,[33–35] PTT/

Correspondence to: T. Kobayashi (toshikazu.kobayashi@usa.dupont.com).

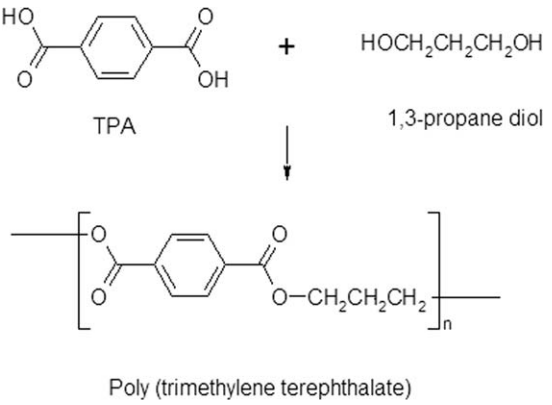

Scheme 1 PTT by condensation reaction from TPA and 1,3-propane diol.

LLDPE,[36,37] and PTT/poly(ether imide) (PEI),[38,39] have been intensively studied. However, very few studies were done for electrical properties for PTT and PTT blends.

Polymers such as polyesters and polyamides are widely used in various fields such as packaging materials, electrical/electronic parts, and automotive parts. However, the static charge that easily builds up on such molded parts from contact/and or rubbing may create the conditions for sparking and cause an electrostatic discharge, which becomes a serious problem because there may be resulting electrostatic damage to sensitive semiconductor devices and interference with circuit operation. To solve those problems, several approaches have been taken for years such as adding low-molecular-weight surfactant or conductive fillers such as carbon black and carbon fiber. More recently, blending ion conductive polymers such as poly(ether esteramide) (PEEA) to create better static dissipative polymer systems was studied.[40–43] We recently confirmed the synergistic effect on electrostatic performance of adding ethylene copolymers based ionomers such as E/MAA-Na and E/MAA-Li into bio-based PTT blends with PEEA. Here, ternary blends of PTT/PEEA/PEG 400 bis (2-ethylhexanoate) (PEG-EH) are investigated in terms of the crystallization, dynamic mechanical properties, morphology, and electrostatic characteristics.

EXPERIMENTAL

Materials

PTT (Sorona® by DuPont, Intrinsic Viscosity: 1.02 dL/g) and PEEA (Pelestat® 6321 $Mw = 84{,}200$) used in this work were commercial polymers manufactured by DuPont, and Sanyo Chemical Corp., respectively. The polymers were used without any purification. Sorona® polymer is manufactured from 1,3-propanediol and DMT on a commercial scale using a continuous polymerization process.[43,44] Pelestat 6321 and PEEA 6500 is confirmed to contain 275 ppm of Na and 3515 ppm of Na, respectively, by inductively coupled plasma (ICP) emission spectrochemical analysis. PEG 400 bis (2-ethylhexanoate) (PEG-EH, $Mw = 652$, Tg: -69°C) was supplied by C.P. Hall Co.

PEEA used here is polymerized from carboxylic acid end nylon 6 oligomer and ethoxylated bisphenol A as shown in Scheme 2. It was identified by ^{1}H-NMR (500 MHz in DMSO-d6) to be composed of PEG/Bisphenol A/Nylon 6/TPA (44.2/6.8/44.1/4.9 in weight %). The chemical structure for PEG-EH is shown in Scheme 3.

Sample preparation

PTT pellets and PEEA pellets were premixed and extruded on a ZSK 30 twin screw extruder using a barrel set temperature of 250°C and a screw speed of 300 rpm with the vacuum vent port applied for all formulations. PEG-EH was added from a liquid injection line from the barrel close to the die. The extruded strand was cut into pellets for injection molding. The extruded pellets were dried for 2 h at 135°C before molding and molded into 7.5 cm × 12.5 cm × 3.2 mm plaques, ASTM tensile test bars and flexural test bars using an injection molding machine (Sumitomo J-150). The set temperatures for the cylinder and the mold were 250°C and 50°C, respectively.

Measurement

Static charge dissipation was measured at 23°C and 50% R.H on Static Honest Meter *S*-4104 (Shishido Shokai Co., Tokyo, Japan) after applying 10 kV of corona discharge for 60 s. Static Honest Meter is a measuring instrument for attenuation of static electricity. This device is used to electrify the specimen by irradiating it by air ions generated by corona discharges initiated by the device, and then, after the irradiation is stopped, it is used to investigate the decay curve of the charge on the specimen. All samples were conditioned with 23°C and 50% R.H. for 48 h prior to the testing. Surface resistivity values were measured according to ASTM D-257.

Transmission electron microscopy (TEM) was performed on ultrathin sections taken from molded tensile bars. To mark the molded surface, the bars were painted with a liquid epoxy mixture which was cured overnight at 60°C. Cryoultramicrotomy with diamond knives was carried out at -90°C to produce sections of nominal thickness 90 nm. Sections were examined both unstained and after 2 h exposure to RuO_4 vapor. Images were obtained

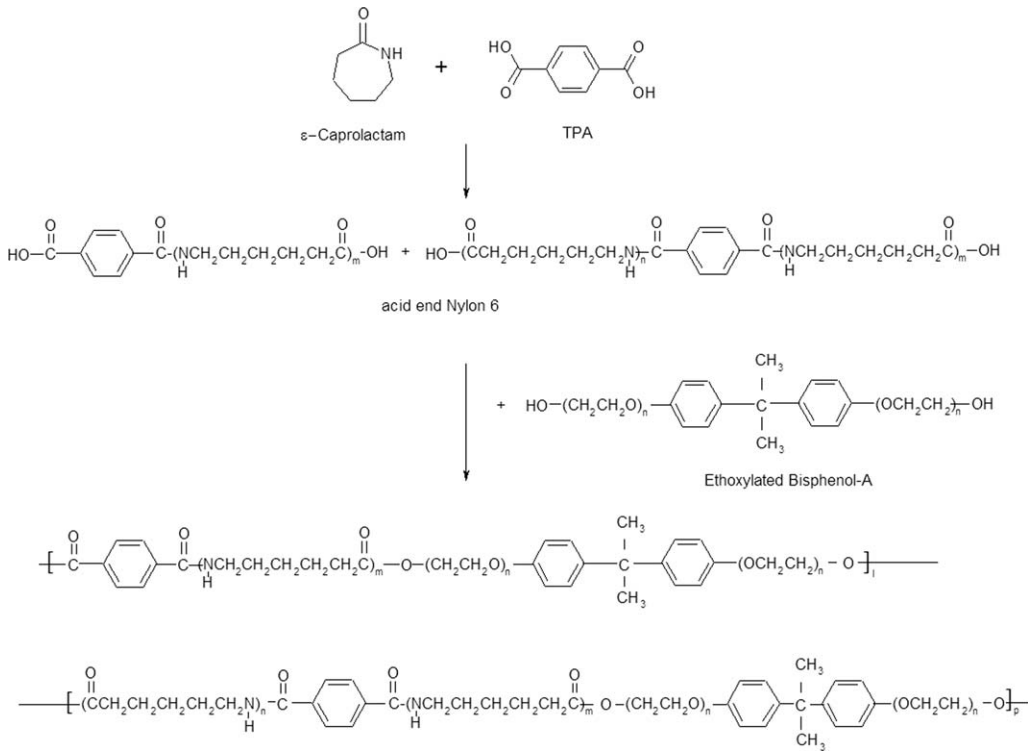

Scheme 2 PEEA by condensation reaction from carboxylic acid end nylon 6 and ethoxylated bisphenol A.

using a JEOL 2000FX TEM operated at 200 KV accelerating voltage and recorded on a digital camera.

The atomic force microscopy (AFM) experiments were performed on a Nanoscope 5/Dimension 5000 from Veeco Metrology. Tapping mode microscopy and optical images were taken of representative regions of the sample and then the cantilever was replaced with a conductive contact mode cantilever for the electrical characterization of the same region. In tunneling AFM (TUNA) a metal coated probe is brought into very light contact with the surface and scanned back and forth. The height is recorded as the probe scans with a feedback loop maintaining a constant deflection of the cantilever. A voltage is applied to the metallic probe and the current is measured at the same time as the height image is collected. It is common practice to switch polarity on the sample to determine if the sign of the current flow changes as expected for a simple resistance.

The sample preparation is important to ensure reliable measurements in conductive or tunneling imaging. The overall resistance of these polymers is high and the signal is near the noise limit of this

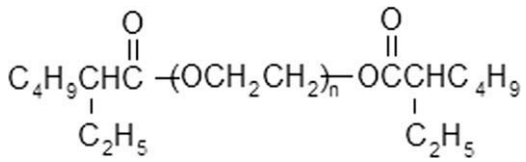

Scheme 3 Polyethylene glycol 400 bis (2-ethylhexanoate).

microscope (1.60×10^{-13} Amps). The sample was cut from an injection molded part and placed into a thin pool of silver conductive paint previously applied to metal pucks. Duco cement was applied at the interface between the bottom of the cut pieces and the pucks to keep them secured during handling. A line of conductive paint was also applied from the top edge of the surface to the metal puck. The silver paint on the front and back of the sample ensures that any conductive pathways are electrically connected through the instrument ground. Regions for imaging were selected at two locations on each sample $\sim$ 150 microns from the edge of the visible paint. At these locations two tunneling AFM images were collected using both a + 10 and −10 V tip bias. Optical images were also captured at the locations.

Dynamic mechanical analysis (DMA) was performed on the samples of 40 mm × 28 mm × 4 mm in size using a dynamic mechanical analyzer (2980 DMA, TA Instruments) under a single cantilever mode in a temperature range from −150 to 150°C at a constant heating rate of 2°C/min, and at frequency of 1 Hz.

A differential scanning calorimeter (DSC), TA Instruments Q1000 MDSC (Modulated DSC) operating in "Standard Mode," was used to determine the cold crystallization and recrystalllization peaks in a melt quenched sample of the thermoplastic composition. A 10–12 mg sample of the composition was weighed into an aluminum DSC pan and the sample heated to 280°C in a DSC for 10 min under nitrogen

TABLE I
Thermal Properties for Various PTT/PEEA Blends

Recipe	Heating				Cooling			
	T_g (°C)	T_{cc} (°C)	ΔH_{cc} (J/g)	T_m (°C)	T_c (°C)	ΔH_c (J/g)	ΔT_c ($T_{onset} - T_c$) (°C)	Crystalline degree (%)
PTT	45.9	72.4	36.5	229.1	172.6	45.4	17.2	31.2
PTT + 12% PEEA-275 Na	44.5	70.4	31.6	228.7	158.6	36.4	27.2	28.4
PTT + 24% PEEA-275 Na	44.2	69.6	29.1	228.1	153.7	32.7	32.0	29.5
PTT + 12% PEEA-3515 Na	44.8	70.7	33.2	228.8	156.0	40.2	29.8	31.4
PTT + 24% PEEA-3515 Na	43.2	69.3	29.2	228.7	160.7	32.1	23.9	29.0
PTT + 3% PEG-EH	35.6	61.0	39.6	227.9	168.0	49.5	19.6	35.0
PTT + 12% PEEA-275 Na + 3% PEG-EH	37.0	60.8	31.3	228.7	157.4	34.2	28.7	27.6
PTT + 24% PEEA-275 Na + 3% PEG-EH	35.0	59.3	30.2	227.5	163.9	36.6	24.0	32.6
PTT + 12% PEEA-3515 Na + 3% PEG-EH	35.8	59.9	32.0	228.3	160.3	41.5	27.2	33.5
PTT + 24% PEEA-3515 Na + 3% PEG-EH	36.5	60.5	31.8	227.7	161.1	36.7	29.0	34.5
PTT + 6% PEG-EH	28.6	–	–	227.5	170.7	50.7	17.6	37.0
PTT + 12% PEEA-275 Na + 6% PEG-EH	35.8	59.2	27.4	228.3	166.5	33.9	20.7	28.4
PTT + 24% PEEA-275 Na + 6% PEG-EH	35.3	51.8	16.6	227.4	167.3	33.8	18.0	33.2
PTT + 12% PEEA-3515 Na + 6% PEG-EH	28.5	48.8	21.2	226.6	164.9	39.4	23.4	30.7
PTT + 24% PEEA-3515 Na + 6% PEG-EH	29.5	47.7	11.8	228.0	165.0	33.2	24.8	32.6

atmosphere to provide an equilibrated melt sample. The melt sample was removed from the DSC and quickly quenched by immersing the sample in liquid nitrogen. The melt quenched sample was equilibrated at 0°C in the DSC under nitrogen atmosphere, followed by heating at 10°C/min scan rate to 280°C; held at isothermal for 3 min at 280°C, and cooled at 10°C/min scan rate to 30°C; while recording the thermal events. The cold crystallization peak (T_{cc}) is the first exothermic peak exhibited in the heating cycle, having a peak height maximum at about 45–75°C. The enthalpy of the recrystallization peak was measured in Joules per gram (J/g). Peak temperatures of the exothermic curves obtained during the cooling scan were defined as the crystallization temperature (T_c). From the exothermic heat of ΔH which is caused by crystallization, the crystallinity is PTT is estimated with the following equation:

$$\text{Crystallinity} = \Delta H/\Delta H^0 \quad (1)$$

where ΔH^0 is the fusion of 100% crystalline polymer. Exothermic heats were normalized by the polymer weight percentage in the crystallinity calculations.

RESULTS AND DISCUSSION

Differential scanning calorimetry

The crystallization rate for PTT and PTT blends studied here can be compared by the crystallizing temperature (T_c) and the half peak width of the crystallization peak (ΔT_c). The higher the T_c peak temperature and the narrower the ΔT_c width are, the faster the crystallization rate is. Table I lists the analyzed values obtained in the DSC measurements for various PTT blends studied here. The heating scan DSC for the quick quenched sample by liquid N2 is shown in Figure 1. The glass transition temperature (T_g) for neat PTT and binary blends of PTT/PEEA is shown around 45°C. Here two kinds of PEEA, low sodium content (275 ppm) and high sodium content (3515 ppm), were investigated. The DSC scan for these PEEA incorporated blends are basically the same. T_g for PTT with 3 and 6% of PEG-EH is shown at 35.9°C and 28.6°C, respectively, which means PEG 400 bis (2-ethylhexanoate) works as a plasticizer for PTT due to its miscibility with PTT.

The cold crystallization peak on heating up to the melt (T_{cc}), which is observed as exothermic peak, was shown at 72.4°C for neat PTT. The exothermic peak enthalpy (ΔH_c) for the various PTT blends are

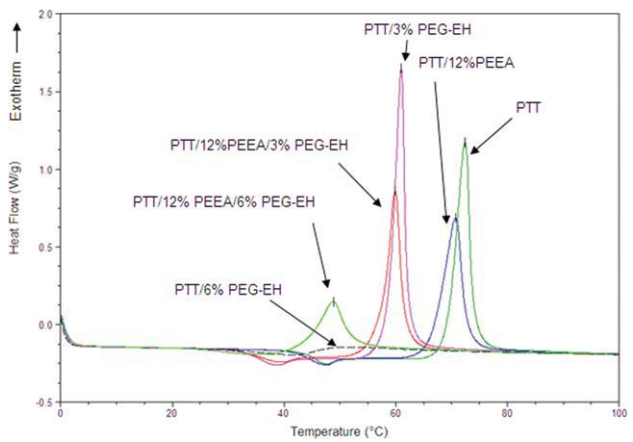

Figure 1 DSC heating scan for PTT blends : PEEA contains 3150 ppm Na. [Color figure can be viewed in the online issue, which is available at wileyonlinelibrary.com.]

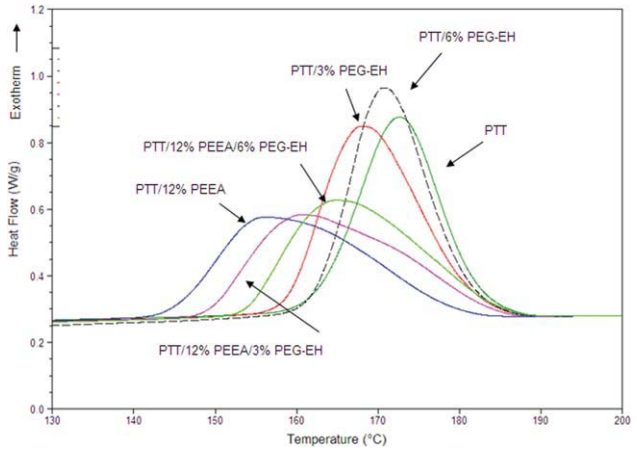

Figure 2 DSC cooling scan for PTT blends : PEEA contains 3150 ppm Na. [Color figure can be viewed in the online issue, which is available at wileyonlinelibrary.com.]

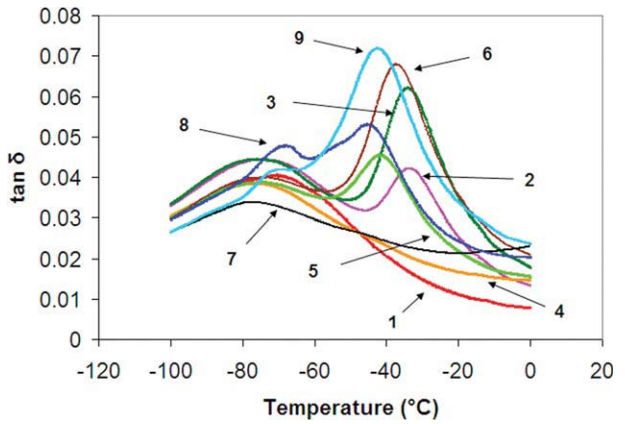

Figure 3 DMA for PTT blends (tan δ versus temperature): −100°Cto 0°C, (1) PTT, (2) PTT/12% PEEA, (3) PTT/24% PEEA, (4) PTT/3% PEG-EH, (5) PTT/12% PEEA/3% PEG-EH, (6) PTT/24% PEEA/3% PEG-EH, (7) PTT/6% PEG-EH, (8) PTT/12% PEEA/6% PEG-EH, (9) PTT/24% PEEA/6% PEG-EH. [Color figure can be viewed in the online issue, which is available at wileyonlinelibrary.com.]

shown in Table I. As shown in Figure 1, PTT with 3% PEG-EH shows T_{cc} at 61.0°C which is about 10°C lower than PTT. This makes sense since T_g for PTT/3% PEG-EH shifted about 10°C lower temperature than neat PTT from DSC scan. When 6% PEG-EH is added into PTT, we do not see any T_{cc} for DSC heating scan, which suggests that PEG-EH gives PTT enough mobility to crystallize during the quenching process by liquid Nitrogen described in the Experimental section. PTT/6% PEG-EH with 10% PEEA, however, shows T_{cc} clearly at 48.8°C which may suggest the part of PEG-EH does not go into PTT matrix due to the existence of PEEA. The interaction of PEEA and PEG-EH is more discussed in Dynamic Mechanical Analysis section.

The cooling scan DSC is shown in Figure 2. The crystallization peak (T_c) for neat PTT can be seen at 172.6°C. When PEEA (3515 ppm Na) is added into PTT, T_c shifts to lower temperature (156.1°C for 10% addition) and the exothermic peak width (ΔT_c : $T_{onset} - T_c$) becomes broader from 17.2°C to 29.8°C, which suggested that PEEA retarded the crystallization rate for PTT and acted as a denucleant. PTT with 6% PEG-EH shows 170.7°C of T_c and 17.6°C of ΔT_c which is similar to those of neat PTT. Although it decreases the T_g of PTT, the crystallization rate of PTT does not seem to change. When PEEA is added into PTT/PEG-EH blends, T_c shifts to lower temperature by 5–10°C and ΔT_c also becomes broader, which is consistent with T_{cc} peak.

The crystallinity for PTT with the previously described DSC conditions was calculated as 31.2% from the cooling scan which has good agreement with Zhang.[45] Normalized crystallinity of the PTT portion for various PTT blends are shown in Table I. The value for ΔH^0 in the eq. (1) is 30 kJ/mol = 145.5 J/g as determined by Pyda et al.[46]

PEEA does not affect on the crystallinity with this cooling condition regardless of the sodium ion content (275 ppm or 3515 ppm). 3 and 6% of PEG-EH in PTT shows 35.0 and 37% crystallinity respectively, which is about 20% higher than for neat PTT.

Dynamic mechanical analysis

Dynamic mechanical heating scan were performed with bars described in experimental section.

Figures 3 and 4 shows tan δ for neat PTT and PTT blends with the temperature range −100°C–20°C, and 0–140°C, respectively. The α-relaxation peak which corresponds to the glass transition temperature for neat PTT is observed at 79.4°C, and the β-relaxation for neat PTT can be observed at −70.4°C. Early studies indicated that β-relaxation is produced by joint movement of phenyl rings and carbonyl entities.[47–51] The β-relaxation for PTT is basically

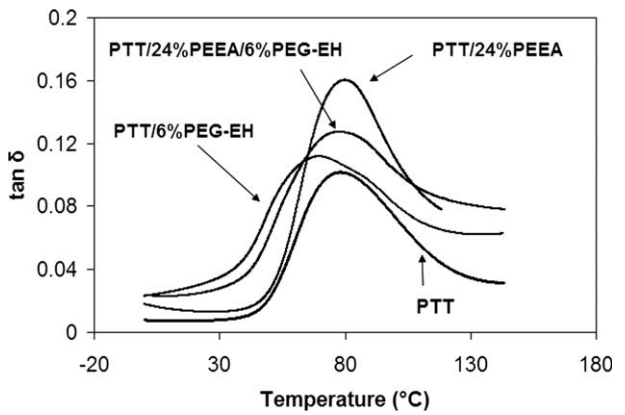

Figure 4 DMA for PTT blends (tan δ versus temperature) : 0 to 140°C.

unchanged when either high ion content PEEA (3515 ppm Na ion) or low ion content PEEA (275 ppm Na ion) is added. The α-relaxation for PTT shifts from 79.4°C to lower temperature of 77.3°C and 70.8°C when PEG-EH content in PTT is increased to 3 and 6%, respectively. T_g for PEG-EH is −69°C, and it works as a plasticizer for PTT due to its miscibility with PTT. However, when PEEA is added into PTT/PEG-EH, the α-relaxation for PTT moves back to 78–80°C range where neat PTT shows its α-relaxation. This means PEG 400 bis (2-ethylhexanoate) (PEG-EH) selectively interact more with PEEA rather than PTT. T_g for PEEA phase in PTT is observed −33.9°C for PTT/12% PEEA (3515 ppm Na) blend, and it moves to −42.1°C, and −45.7°C when the amount of PEG-EH into PTT/12% PEEA increases to 3%, and 6%. And T_g for PEEA phase in PTT is observed −34.0°C for PTT/24% PEEA(3515 ppm Na) blend, and it shifts to −37.4°C, and −42.5°C when the amount of PEG-EH into PTT/24% PEEA increases to 3 and 6%.

There is no separate α-relaxation peak for PEG-EH for ternary blend of PTT/PEEA/PEG-EH. In addition to this DMA result, because both PEEA and PEG-EH contain polyethylene glycol segment in the molecular backbone, they are a miscible pair. Although it may not be appropriate to draw the T_g curve for the PEEA and PEG-EH weight ratio from the ternary blends DMA results, still it seems worth making a graph for the T_g as shown in Figure 5, where the X axis is the weight ratio of PEEA/PEG-EH. Several models have been proposed to predict the composition dependence of T_g in the miscible polymer blends. Some of these are Couchman,[52] Fox,[53] Gordon–Taylor,[54] and Utracki,[55] equations. In the Fox model, the observed T_g of the blend is related to the T_g values of the neat components and their composition according to the following equation:

$$\frac{1}{T_g} = \frac{W_1}{T_{g1}} + \frac{W_2}{T_{g2}} \tag{2}$$

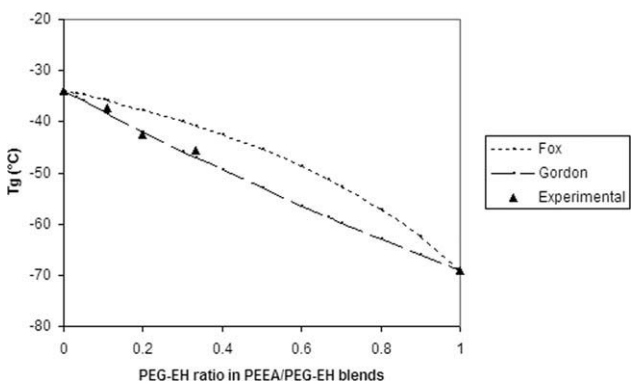

Figure 5 T_g prediction of PEEA/polyethylene glycol 400 bis(2-ethylhexanoate).

where W_1 and W_2 are the weight fraction of the components 1 and 2 having the T_g values of T_{g1} and T_{g2}, respectively. The Gordon–Taylor equation for the prediction of the composition dependence of T_g in miscible polymer blends is written as:

$$T_g = \frac{W_1 T_{g1} + k W_2 T_{g2}}{W_1 + k W_2} \tag{3}$$

where k is the fitting parameter.

Figure 5 shows the experimental data for the T_g of the blends corresponding to PEEA domain as obtained from the DMA data along with the predictions of the Fox model and the Gordon–Taylor equation with a fitting parameter of $k = 1.2$. It is clearly observed from Figure 5 that the Gordon–Taylor equation fits the experimental data better than the Fox equation.

One of the unique characteristics of the PTT blends with PEEA is their electrostatic dissipative performance due to the ion conductive nature of PEEA. Here, we investigated two kinds of PEEA, high ion content (3515 ppm Na ion) and low ion content (275 ppm Na ion). The T_g of the PEEA domains also influences its electrostatic performance, which is discussed in the electrical properties section below.

Surface charge decay

PEEA is known as an ion conductive polymer and is commercially available as a polymeric additive to add antistatic characteristics to polymers. We previously investigated electrostatic decay performance for PET/PEEA blends with various ethylene polymers. We found that the static decay performance for PET/PEEA blends can be drastically improved by adding E/MAA-Li and E/MAA-Na. Here we investigate bio-based PTT/PEEA with PEG-EH. Surface charge decay curves up to 60 s for the samples were obtained by Static Honest Meter S4104 after applying 10 kV of corona discharge for 1 min. This device is used to electrify the specimen by irradiating it with air ions generated by corona discharges initiated by the device. After the irradiation is stopped, it is used to investigate the decay curve of the charge on the specimen. Static charge dissipation curve for neat PTT and PTT blend with high ion content PEEA and low ion content PEEA are shown in Figure 6. Neat PTT shows no dissipation during measured time of 60 s. The surface charge for PTT/12% low ion content PEEA drops from 2120 V to 120 V in 60 s. PTT/12% high ion content PEEA shows much faster electrostatic dissipation with reaching 110 V in only10 s. 24% of high ion PEEA in PTT also gives faster electrostatic dissipation than 24% of low ion content PEEA. PEEA works effectively to add static dissipative

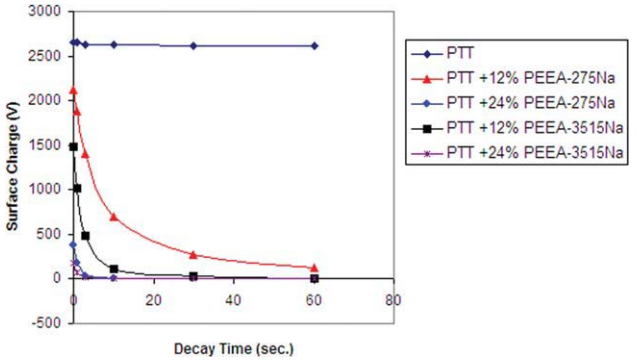

Figure 6 Electrostatic charge decay for PTT and PTT/PEEA (275 ppm ion,3515 ppm ion). [Color figure can be viewed in the online issue, which is available at wileyonlinelibrary.com.]

characteristics to PTT through the ion conductive nature of PEEA. The higher the ion content in PEEA, which is an ion conductive polymer, the faster the electrostatic dissipation is achieved. Figure 7 shows electrostatic decay for PTT/24% PEEA with 3 and 6% PEG-EH. PEG-EH effectively works to enhance the electrostatic dissipation for PTT/PEEA blends probably due to increased ion mobility by decreasing the glass transition temperature of PEEA.

Static decay performance index

Matsui and Kashiwamura studied the relationship between resistivity, frictional charge, and half dissipation time for antistatic fabricated fiber.[56] In their report, a concept of Index of frictional static charge dissipation was proposed to describe the antistatic performance more appropriately. It is integral of the charge dissipation curve up to 1 min after the applied friction, which is, in other words, the average static charge during 1 min multiplied by 1 min as described in eq. (4) and (5). It is known that the dissipation speed decreases when the surface charge becomes small even for the same material. Therefore, half dissipation time tends to become larger when initial surface charge of the material is low. Since good antistatic material tends to have lower initial surface charge with the same applied corona discharge, half dissipation time of the material does not always represent the antistatic performance appropriately, which sometimes makes it difficult to differentiate excellent antistatic material from others. This index is considered as a new method to describe the antistatic performance from the standpoint of both initial surface charge and decay curve.

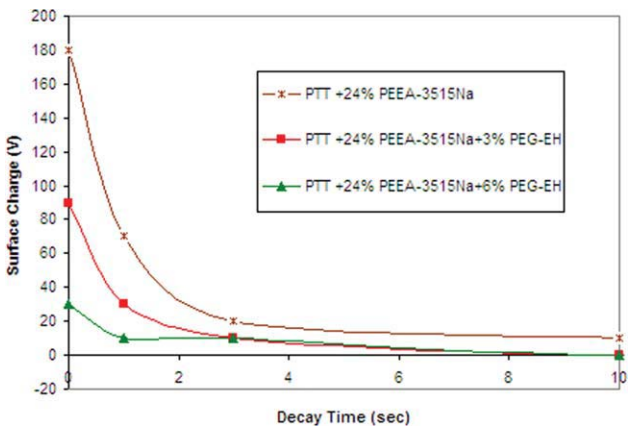

Figure 7 Electrostatic charge decay for PTT/PEEA-3515Na/PEG bis(2-ethylhexanoate). [Color figure can be viewed in the online issue, which is available at wileyonlinelibrary.com.]

We previously applied the Matsui and Kashiwamura concept for describing static charge dissipation to discuss a broader aspect and confirmed the effectiveness of static decay performance index (SDPI).[42] The lower the SDPI value, the better static dissipative performance is achieved.

$$V = f(t) \tag{4}$$

$$\mathrm{SDPI} = \int_0^1 f(t)dt \tag{5}$$

Table II shows the SDPI for the PTT with PEG-EH when the PEEA content is 12%. With increasing PEG-EH content, the SDPI goes down for both high ion content PEEA and low ion content PEEA since it enhances the ion mobility by reducing the glass transition temperature of PEEA. High ion content PEEA gives a much smaller SDPI than low ion PEEA. PTT/24% PEEA (3515 ppm Na) has 8.5×10^9 Ω/sq of surface resistivity versus 5.1×10^{10} Ω/sq for

TABLE II
Surface Resistivity and Static Decay Performance Index (SDPI) for PTT blends

	Surface resistivity (Ω/sq)	SDPI (V min)
PTT	2.2E+15	2624
PTT + 12% PEEA-275 Na	1.7E+12	470
PTT + 24% PEEA-275 Na	5.1E+10	12
PTT + 12% PEEA-3515 Na	2.4E+11	111
PTT + 24% PEEA-3515 Na	8.5E+09	7
PTT + 3% PEG-EH	2.0E+13	1656
PTT + 12% PEEA-275 Na + 3% PEG-EH	1.0E+12	341
PTT + 24% PEEA-275 Na + 3% PEG-EH	3.6E+10	16
PTT + 12% PEEA-3515 Na + 3% PEG-EH	4.7E+10	30
PTT + 24% PEEA-3515 Na + 3% PEG-EH	4.8E+09	2
PTT + 6% PEG-EH	5.0E+13	1246
PTT + 12% PEEA-275 Na + 6% PEG-EH	6.4E+11	150
PTT + 24% PEEA-275Na + 6% PEG-EH	2.3E+10	8
PTT + 12% PEEA-3515 Na + 6% PEG-EH	4.8E+10	18
PTT + 24% PEEA-3515 Na + 6% PEG-EH	2.4E+09	1

PTT/24% PEEA(275 ppm Na) With 6% PEG-EH, PTT/24% PEEA(3515 ppm Na) shows 2.4×10^9 Ω/sq and PTT/24% PEEA(275 ppm Na) shows 2.3×10^{10} Ω/sq, which is consistent with all the electrostatic results. It is very clear that PEG-EH enhances the antistatic performance of PTT/PEEA. Complete data for surface resistivity and SDPI is shown in Table II.

Morphology (TEM)

In our previous study, we found E/MAA acid copolymer without any metal cation works as a synergist for PET/PEEA blends, which suggests that the mechanism of the antistatic synergist is not ion transfer from the ionomer to PEEA but rather morphological interaction in which the PEEA encapsulates dispersed domains of the third polymer.[42] The E/MAA copolymer is seen as a discrete dispersed phase in TEM images. Encapsulation results in higher surface area/per unit volume of PEEA compared to PET/PEEA binary blends. Here we found PEG-EH improves the antistatic performance for PTT/PEEA blends by decreasing the T_g of PEEA which leads to enhance the ion mobility in the PEEA. No separate PEG-EH phase was detected in the images, which is to be expected if the PEG-EH acts as a miscible plasticizer for the PTT matrix, but this do not rule out a single mixed dispersed phase of PEEA and PEG. For the binary PTT/PEEA blend, the surface morphology of molded specimens is layerlike, but the layers are longer and thicker for the higher Na grade of PEEA [Fig. 8(a,b)].

According to the PEEA manufacturer's information, the melt index of both grades is the same, so viscosity differences are not a likely explanation for the morphology difference.

Comparing the two grades of PEEA used in combination with PTT and PEG-EH, we see no difference in the subsurface morphology near the center of molded specimens [Fig. 8(c,d)]. At the molded surface, however, the morphology changes from layerlike [Fig. 8(e)] to a finer weblike dispersion [Fig. 8(f)] on changing from PEEA with 275 ppm to 3315 ppm Na. This suggests that the ternary blend morphology is shear sensitive, yielding molded bars that are very similar in structure in the center but with different features at the molded surface according to PEEA type. The superior SDPI performance of high Na PEEA formulations may be in part attributable to the superior dispersion of the ion-rich species at the molded surface of parts.

Atomic force microscopy

The layered surface structure revealed in TEM images of the ternary blend PTT/PEEA/PEG-EH is also evident in AFM images of the surface of the molded plaque. Figure 9 shows that a striated structure is present in phase images of both the binary blend of PTT with 12% PEEA [9(a)] and the ternary blend with 12% PEEA and 6% PEG-EH [9(b)]. This oriented direction corresponds to the mold flow direction. Figure 9(b) shows broader striated PEEA domain which enhances the static dissipation. Figure 9(c,e) are the topographic image for the same sample of 9(a,b), respectively. Similar pattern can be seen between phase image and topographic image for both PTT/12% PEEA and PTT/12% PEEA/6% PEG-EH samples. Figure 9(d,f) show tunneling AFM (TUNA) for the same sample location of 9(c,e), respectively. In TUNA, only the ternary blend, Figure 9(f), shows the striated structure indicative of conductive pathways which seem to correspond darker color striated pattern of topographic image of Figure 9(e). For this TUNA image applied with + 10 V tip bias, brighter color means more conductive than darker color area as indicated by the image bar in the picture. Figure 9(d) does not show any conductivity at all. On the other hand, 9(f) shows much brighter color for the whole area and shows the striated structure indicative of more conductive pathways. TUNA image suggests the whole surface area becomes more electrostatically dissipative since the entire area is covered with a brighter color. The SDPI value for the sample 9(d) is 111 V min and that for sample 9(f) is 18 V min. It is confirmed that good static dissipative material with low SDPI value can be observed by TUNA. Although the striated phase and TUNA current images resemble the TEM images in some respects, they are not really sampling the same orientation. It must be remembered that the AFM images are surface images, while the TEM images are cross sections.

CONCLUSIONS

Bio-based PTT and PTT blends with PEEA of different ion content (275 ppm Na and 3515 ppm Na) and PEG 400 bis (2-ethylhexanoate) (PEG-EH) were studied in terms of the crystallization, dynamic mechanical properties, multicomponent morphology by TEM and AFM and electrical characteristics. DSC and DMA suggest that PTT and PEG-EH is miscible at least up to 6% in PTT where the blend range is studied here. PEG -EH works as a plasticizer for PTT. In case of ternary blends of PTT/PEEA/PEG-EG, PEG-EH selectively goes into PEEA phase rather than PTT phase and PEG-EH and PEEA is a miscible pair, and the Gordon–Taylor equation fits the observed T_g of PEEA/PEG-EH.

SDPI, a convenient figure of merit for comparing different polymeric materials, was calculated from

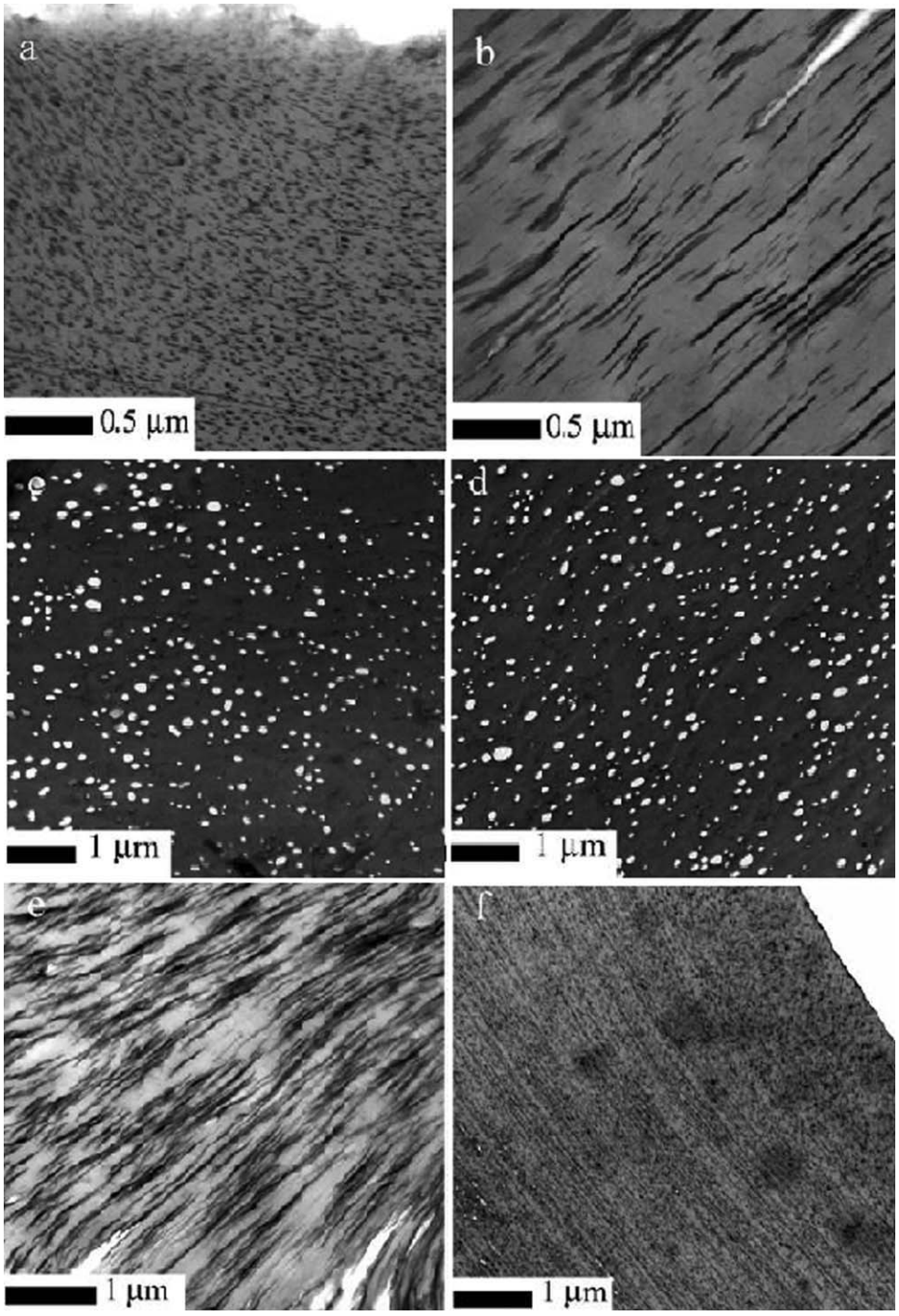

Figure 8 TEM of PTT blends: surface cross section: (a) PTT/12% PEEA (275 ppm-Na), (b) PTT/12% PEEA (3515 ppm-Na), core cross section: (c) PTT/12% PEEA(275 ppm-Na)/6% PEG-EH, (d)PTT/12% PEEA(3515 ppm-Na)/6% PEG-EH, surface cross section: (e) PTT/12% PEEA(275 ppm-Na)/6% PEG-EH, (f)PTT/12% PEEA(3515 ppm-Na)/6% PEG-EH.

the electrostatic dissipation curve and it was confirmed that PEEA works effectively to reduce the SDPI for PTT. High ion content PEEA shows much smaller SDPI than low ion content PEEA. PEG-EH improves the electrostatic dissipative performance by enhancing the ion mobility in PEEA domains through reducing the glass transition temperature of PEEA which is an ion conductive polymer.

PTT/PEEA/PEG-EH blends show layered elongated domain structure for the close to the surface. High Na content PEEA with PEG-EG shows very fine layered domains with about 10 nm thickness whereas about 100 nm size particles are observed at cross section of core part. Tunneling AFM was used to observe the surface morphology of the static dissipative materials, and it enabled us to directly map

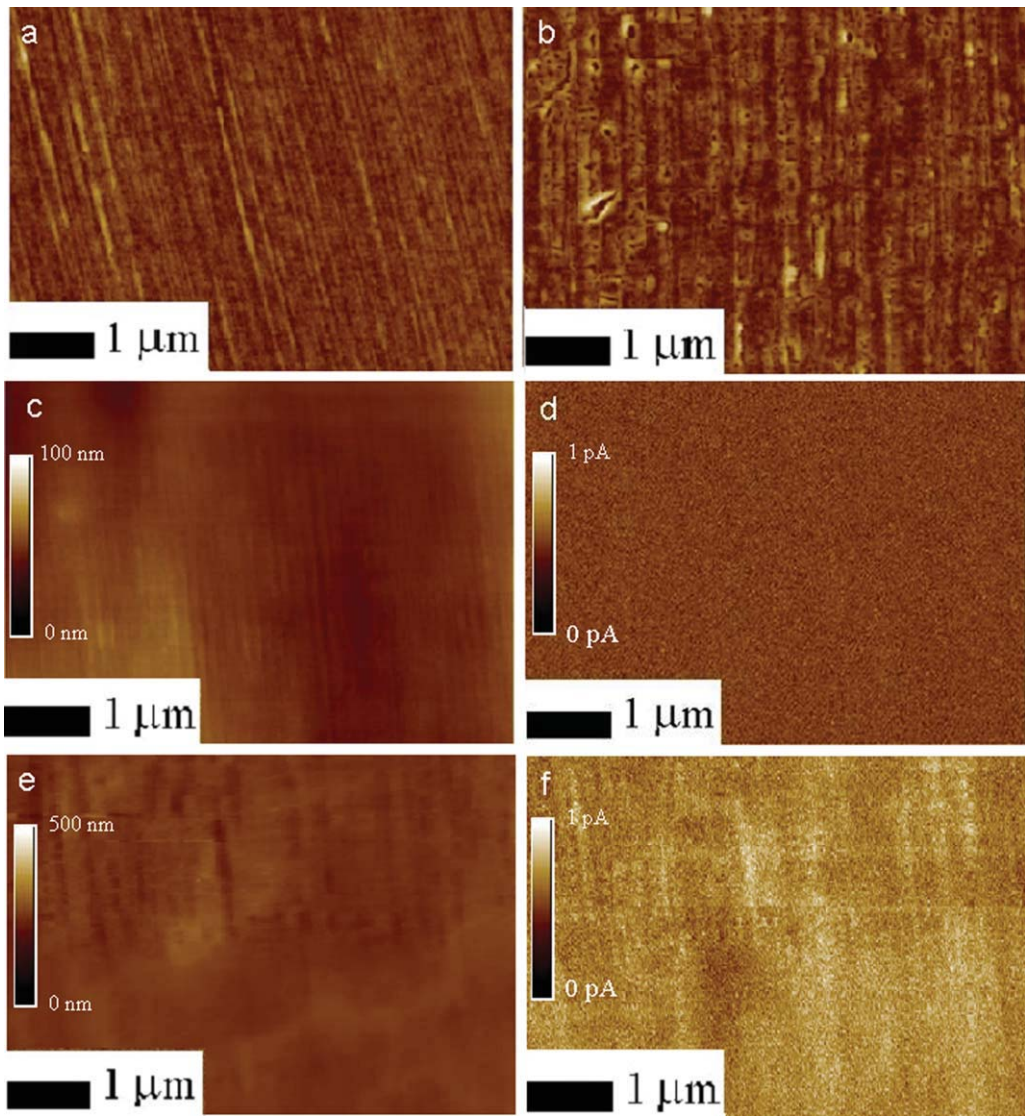

Figure 9 AFM phase image: (a) PTT/12% PEEA, (b) PTT/12% PEEA/6% PEG-EH, topographic image: (c) PTT/12% PEEA, (e) PTT/12% PEEA/6% PEG-EH, Tunneling AFM: (d) PTT/12% PEEA, (f) PTT/12% PEEA/6% PEG-EH All of PEEA used here contain 3515 ppm Na ion. [Color figure can be viewed in the online issue, which is available at wileyonlinelibrary.com.]

the electro-conductive pathways on the surface of the molded sample.

The authors sincerely thank Dave Gale, DuPont Engineering Polymers, and Yukio Miyagishima, Engineering Polymers Research, DuPont K. K. for the DSC and DMA measurement and Don Brill for the AFM imaging, and NMR analysis for Dr. Elizabeth Lozada in Corporate Center for Analytical Solutions at DuPont.

References

1. Emptage, M.; Haynie, S.; Laffend, L.; Pucci, J.; Whited, G. Eur. Pat. EP 1,204,755 (2001).
2. Whited, G. M.; Bulthuis, B.; Trimbur, D. E.; Gatenby, A. A. Eur. Pat. EP 1,076,708 (1999).
3. Burch, R. R.; Dorsch, R. R.; Laffend, L. A.; Nagarajan, V. Int. Pat. WO 0,111,070 (2001).
4. Kurian, J. V. J Polym Environ 2005, 13, 159.
5. Grebowicz, J. S.; Brown, H.; Chuah, H. H.; Olvera, J. M.; Wasiak, A.; Sajkiewicz, P. Polymer 2001, 42, 7153.
6. Wu, J.; Schultz, J. M.; Samon, J. M.; Pangelinan, A. B.; Chuah, H. H. Polymer 2001, 42, 7161.
7. Wu, G.; Li, H. W.; Wu, Y. Q.; John, A. C. Polymer 2002, 43, 4915.
8. Shu, Y. C.; Hsiao, K. J. Eur Polym J 2006, 42, 2773.
9. Ho, R. M.; Ke, K. Z.; Chen, M. Macromolecules 2000, 33, 7529.
10. Wang, B. J.; Christopher, Y. L.; Jennifer, H.; Stephen, Z. D. C.; Phillip, H. G. Polymer 2001, 42, 7171.
11. Chen, M.; Chen, C. C.; Ke, K. Z.; Ho, R. M. J Macromol Sci Phys 2002, 41, 1063.
12. Yun, J. H.; Kuboyama, K.; Chiba, T.; Ougizawa, T. Polymer 2006, 47, 4831.
13. Chung, W. T.; Yeh, W. J.; Hong, P. D. J Appl Polym Sci 2002, 83, 2426.
14. Chuah, H. H. Polym Eng Sci 2001, 41, 308.
15. Hong, P. D.; Chung, W. T.; Hsu, C. F. Polymer 2002, 43, 3335.
16. Srimoaon, P.; Dangseeyun, N.; Supaphol, P. Eur Polym J 2004, 40, 599.

17. Chuang, W. T.; Hong, P. D.; Chuah, H. H. Polymer 2004, 45, 2413.
18. Xue, M. L.; Yu, Y. L.; Sheng, J.; Chuah, H. H. J Macromol Sci Polym Phys 2005, 44, 531.
19. Xue, M. L.; Sheng, J.; Yu, Y. L.; Chuah, H. H. Eur Polym J 2004, 40, 811.
20. Liu, Z.; Chen, K.; Yau, D. Eur Polym J 2003, 39, 2359.
21. Ou, C. F. J Polym Sci Part B: Polym Phys 2003, 41, 2902.
22. Liu, Z.; Chen, K.; Yau, D. Polym Test 2004, 23, 323.
23. Mishra, J. K.; Chang, Y. W.; Choi, N. S. Polym Eng Sci 2007, 47, 863.
24. Xu, Y.; Jia, H. B.; Piao, J. N.; Ye, S. R.; Huang, J. J Mater Sci 2008, 43, 417.
25. Chung, G. S.; Choi, K. R.; Lin, K. Y.; Kim, B. C. Polym Mater Sci Eng 2001, 84, 501.
26. Kuo, Y. H.; Woo, E. M. Polym J 2003, 35, 236.
27. Supaphol, P.; Dangseeyun, N.; Thanomkiat, P.; Nithitanakul, M. J Polym Sci Part B: Polym Phys 2004, 42, 676.
28. Supaphol, P.; Dangseeyun, N.; Srimoaon, P.; Nithitanakul, M. Polym Test 2004, 23, 175.
29. Xue, M. L.; Sheng, J.; Chuah, H. H.; Zhang, X. Y. J Macromol Sci Phys 2004, 43, 1045.
30. Lee, L. T.; Woo, E. M. Colloid Polym Sci 2004, 282, 1308.
31. Oh, S. J.; Chae, D. W.; Lee, H. J.; Kim, B. C. Polym Mater Sci Eng 2001, 84, 621.
32. Bae, W. J.; Jo, W. H.; Park, Y. H. Macromol Res 2002, 10, 145.
33. Ravikumar, H. B.; Raganathaiah, C.; Kumaraswamy, G. N.; Thomas, S. Polymer 2005, 46, 2372.
34. Aravind, I.; Albert, P.; Ranganathaia, C.; Kurian, J. V.; Thomas, S. Polymer 2005, 45, 4925.
35. Ravikumar, H. B.; Ranganathaiah, C. Polym Int 2005, 54, 1288.
36. Jafari, S. H.; Asadinezhad, A.; Yavari, A.; Khonakdar, H. A.; Bohme, F. Polym Bull 2005, 54, 417.
37. Jafari, S. H.; Yavari, A.; Asadinezhad, A.; Khonakdar, H. A.; Bohme, F. Polymer 2005, 46, 5082.
38. Kuo, J. M.; Woo, E. M.; Kuo, T. Y. Polym J 2001, 33, 920.
39. Huang, J. M.; Chang, F. C. J Appl Polym Sci 2002, 84, 850.
40. Fukunaga, K.; Maeno, T. J. Electrostatics 1997, 40/41, 431.
41. Kobayashi, T.; Wood, B. A.; Takemura, A.; Ono, H. J Electrostatics 2006, 64, 377.
42. Kobayashi, T.; Wood, B. A.; Takemura, A.; Ono, H. Polym Eng Sci 2008, 48, 2247.
43. Chang, J. C.; Kurian, J. V.; Miller, R. W. U.S. Pat. 7,033,530 (2006).
44. Giardino, C. J; Griffith, D. B.; Ho, C.; Howell, J. M.; Watkins, M. H.; Duffy, J. J. U.S. Pat.6,353,062 (2002).
45. Zhang, J. J. Appl Polym Sci 2004, 91, 1657.
46. Pyda, M.; Boller, A.; Grebowicz, J.; Chuah, H.; Lebedev, B. V.; Wunderlich, B. J Polym Sci Part B: Polym Phys 1998, 36, 2499.
47. Gonzalez, C. C.; Perena, J. M.; Bello, A. J Polym Sci Part B: Polym Phys 1988, 26, 1397.
48. Kalakkunnath, S.; Kalika, D. S. Polymer 2006, 47, 7085.
49. Mackintosh, A. R.; Liggat, J. J. J Appl Polym Sci 2004, 92, 2791.
50. Maxwell, A. S.; Monnerie, L.; Ward, I. M. Polymer 1998, 39, 6851.
51. Corrales, T.; Peinado, C.; Bosch, P.; Catalina, F. Polymer 2004, 45, 1545.
52. Couchman, P. R.; Karasz, F. E. Macromolecules 1978, 11, 117.
53. Fox, T. G. Bull Am Phys Soc 1956, 2, 123.
54. Gordon, M.; Taylor, J. S. J Appl Chem 1952, 2, 493.
55. Utracki, L. A. Adv Polym Technol 1985, 5, 33.
56. Matsui, M.; Kashiwamura, T. Sen-I Gakkaishi 1993, 49, 421.